

Charles University in Prague  
Faculty of Mathematics and Physics  
and  
AGH - University of Science and Technology  
Faculty of Physics and Applied Computer Science

Damian Rybicki

*Nuclear magnetic resonance study of selected  
Ruddlesden-Popper manganites*

Abstract of doctoral thesis  
Branch F3 – Physics of Condensed Matter and Material Research

2007

## Contents

1. Introduction.....	2
2. Properties of “cubic” and bilayered manganese perovskites .....	3
3. Nuclear Magnetic Resonance.....	4
4. Magnetometers and NMR spectrometers.....	4
5. Experimental results and discussion.....	5
5.1 $\text{La}_{0.875}\text{Sr}_{0.125}\text{MnO}_3$ and $\text{La}_{0.85}\text{Sr}_{0.15}\text{MnO}_3$ $^{55}\text{Mn}$ and $^{139}\text{La}$ NMR.....	5
5.2 Nanoparticles of $\text{La}_{0.75}\text{Sr}_{0.25}\text{MnO}_3$ .....	11
5.3 Bilayered manganese perovskites, $\text{La}_{2-2x}\text{Sr}_{1+2x}\text{Mn}_2\text{O}_7$ .....	14
6. Conclusions.....	22
7. List of publications.....	23
8. References.....	25

## 1. Introduction

“Cubic” and bilayered manganese perovskites belong to a very broad family of oxide compounds of transition metals crystallizing in the perovskite structure. They are a part of the Ruddlesden-Popper phases system which is described by the formula:  $(A_{1-x}B_x)_{n+1}Mn_nO_{3n+1}$ , where  $A$  and  $B$  are trivalent and divalent cations, respectively. The compounds studied exhibit intriguing magnetic and electronic properties and phenomena, including phase segregation. They also show magnetoresistance effect, which is very promising in terms of possible applications. Magnetic and electronic properties of these compounds are closely interrelated, due to the same ( $d$ ) character of the “magnetic” and “conduction” electrons. The interplay of lattice, charge, spin and orbital degrees of freedom results in a variety of electronic and magnetic properties ranging from a metallic or insulating ferromagnetic (FM), to antiferromagnetic (AF) insulating, or paramagnetic insulating behaviour. Manganese perovskites offer a unique opportunity to study and verify concepts introduced by theoretical physicists and chemists, which can also be very useful in other fields of physics.

In this work the effect of “dimensionality” of the compounds’ structure is studied. “Cubic” manganese perovskites with general formula  $(A_{1-x}B_x)MnO_3$  are considered as three dimensional compounds, while bilayered perovskites,  $(A_{1-x}B_x)_3Mn_2O_7$  are considered as (quasi) two dimensional. Other important aspects and factors which influence properties of these compounds are also studied, such as: the effect of Sr or Ca doping, the influence of the grain size on the magnetic and electronic properties and how the applied magnetic field affects the local properties. Additionally, for some compounds the temperature changes of their properties are investigated. Namely, an attempt is made to check if the phase segregation picture is a common feature for various manganese perovskites, which differ in terms of their macroscopic properties.

In order to study local properties of the compounds of interest, the Nuclear Magnetic Resonance (NMR) method was employed and complemented with bulk magnetic measurements.

## 2. Properties of “cubic” and bilayered manganese perovskites

The compounds studied belong to the Ruddlesden-Popper phases with a general formula  $(A_{1-x}B_x)_{n+1}Mn_nO_{3n+1}$ , the  $n$  parameter can be equal to 1, 2, 3,... and  $\infty$ ,  $x$  is the doping,  $A$  is a trivalent cation and  $B$  is a divalent cation. When  $n=\infty$  one obtains the formula  $(A_{1-x}B_x)MnO_3$  of so called three dimensional “cubic” perovskites. If  $n=2$  the general formula is  $(A_{1-x}B_x)_3Mn_2O_7$ , compounds from this series are sometimes referred as two dimensional bilayered perovskites, which is due to their quasi two dimensional crystallographic structure.

Mixed valence manganese perovskites of the general formula  $(A_{1-x}B_x)MnO_3$  became for the first time the subject of interest of physicists in the fifties of the last century [Jonker 1950, 1956, van Santen 1956]. When  $A^{3+}$  is substituted with  $B^{2+}$  with oxygen ion maintaining  $O^{2-}$  state, the relative fraction of  $Mn^{3+}$  to  $Mn^{4+}$  decreases with increasing doping  $x$ . The interest in manganites revived in the 1990s, when large magnetoresistance (MR) effects were found in  $Nd_{0.5}Pb_{0.5}MnO_3$  [Kusters 1989].

For understanding the physics related to manganese perovskites it is also essential to consider possible magnetic interactions between  $Mn$  ions i.e. the super-exchange (SE) and double exchange (DE) interactions. The SE interaction occurs between two magnetic ions of the same valence through the occupied oxygen  $2p$  orbital (Fig. 1). The SE interaction is a virtual exchange between electrons of magnetic ions with electrons from the same  $2p$  orbital of oxygen, which have antiparallel spins according to Pauli exclusion principle. Therefore the orientation of spins of magnetic ions is also antiparallel and leads to AF ordering of the material. Since SE is only “virtual” exchange it does not affect the mobility of electrons.

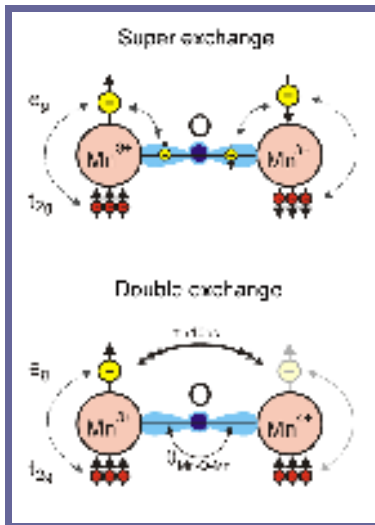


Fig. 1 The schematic diagram of mechanism of the double exchange and super-exchange interactions in the case of two  $Mn$  cations.

The DE interaction occurs between two  $Mn$  ions of different valence also through the  $2p$  oxygen orbital, but unoccupied (Fig. 1). The DE interaction occurs when the electron from the  $e_g$  orbital (of  $Mn^{3+}$  ion) can hop to a neighbouring site (to  $Mn^{4+}$  ion), when there is a vacancy of the same spin [Zener 1951]. As a result of the first Hund’s rule and strong exchange interaction of the  $e_g$  electron and three  $t_{2g}$  electrons all electron spins are aligned. Therefore the hopping of the  $e_g$  electron from one site to other site with  $t_{2g}$  electron spins antiparallel to the  $e_g$  electron spin is not energetically favourable. As a result, ferromagnetic alignment of neighbouring magnetic ions is required to maintain the high spin state of both ions. Another result of electron hopping is the appearance of itinerant electrons in the system, which results in metallicity of the material.

Due to the strong competition between the DE and SE interactions and electron-phonon interactions (i.e. Jahn-Teller effect) in manganites a rich variety of possible types of magnetic (paramagnetic, FM, AF, canted AF) and electronic (metallic, insulating) phases can occur. Moreover, in manganites ferromagnetic metallic (FMM) phase can coexist with ferromagnetic insulating (FMI) or antiferromagnetic insulating (AFI) phases. Also charge order ( $Mn^{3+}$  and  $Mn^{4+}$  ions) and orbital order of the  $Mn^{3+}$   $3d$   $e_g$  orbitals ( $d_{x^2-y^2}$  or  $d_{3z^2-r^2}$ ) are

possible.

### 3. Nuclear Magnetic Resonance

Nuclear magnetic resonance (NMR) uses nuclear magnetic dipole moments and electric quadrupole moments as “local” probes of electronic and magnetic states of their parent atoms with the selectivity to the individual isotope of the element. Nuclear magnetic dipoles probe magnetic hyperfine fields produced by electrons and the nuclear electric quadrupoles probe electric field gradients produced by an electric charge density of aspherical distribution around the nucleus. It provides the information on the magnetic and electronic state of an element at the individual structural and magnetic sites. Fluctuations of the hyperfine fields and electric field gradients contribute to the nuclear relaxation. Performing the NMR experiment in an applied magnetic field enables us to study the local arrangement of magnetic moments and their coupling.

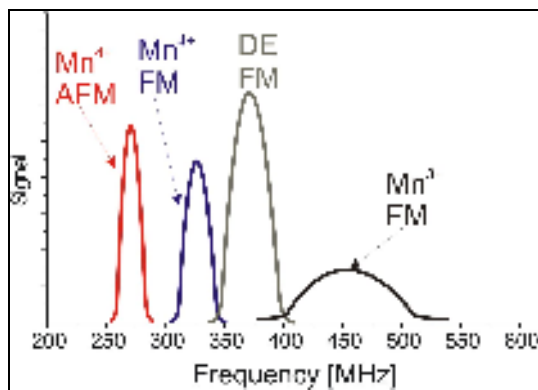


Fig. 2. Schematic plot of the frequency swept  $^{55}\text{Mn}$  NMR spectrum with possible resonant lines and their attribution to various phases.

NMR measurements also revealed electronic phase separation in manganese perovskites [Allodi 1997, Papavassiliou 1999, 2000, Renard 1999, Kapusta 2000a, 2000b]. Phase separation observed with the NMR method manifests itself with distinct resonant lines in the spectra. Resonances of  $^{55}\text{Mn}$  nuclei around 330 MHz or higher than 400 MHz are due to  $\text{Mn}^{4+}$  and  $\text{Mn}^{3+}$  ions in the FMI phase. Signals between 250-290 MHz are due to the resonance of  $\text{Mn}^{4+}$  ions in the AFI phase. The resonance around 370-380 MHz is due to manganese ions with intermediate valence (between 3+ and 4+) as a result of the ferromagnetic coupling resulting from the DE interaction [Matsumoto 1970]. Observation of this resonance indicates that the characteristic time of electron hopping due to the DE interaction is shorter than the difference in precession periods of the nuclear magnetic moment in the two states (3+ and 4+) of an ion when the direction of hyperfine field does not change, i.e.  $\ll 5 \cdot 10^{-9}\text{s}$ . A schematic plot of the frequency swept spectrum with possible resonant lines is presented in Fig. 2. In [Allodi 1997] results of  $^{55}\text{Mn}$  and  $^{139}\text{La}$  NMR measurements, showed coexistence of AF and FM subsystems in *Ca* doped *LaMnO<sub>3</sub>* compounds. Coexistence of FMM and FMI regions is also possible as was concluded for low doped *La<sub>1-x</sub>Sr<sub>x</sub>MnO<sub>3</sub>* system [Renard 1999].

### 4. Magnetometers and NMR spectrometers

In this thesis the results of magnetic measurements carried out on the Vibrating Sample Magnetometer and the SQUID (superconducting quantum interference device) magnetometer and NMR measurements carried out on two spectrometers are presented. The NMR spectrometer at the Faculty of Physics and Applied Computer Sciences of AGH-University of Science and Technology in Krakow is a “home made” spectrometer and the spectrometer at the Faculty of Mathematics and Physics of Charles University in Prague is an adapted Bruker AVANCE high-resolution spectrometer. NMR frequency swept spectra are

obtained by the spin echo method. Both spectrometers consist of:

- the pulse generator, with the splitters and the power amplifier in the transmitter section,
- the receiver section, with the signal amplifiers, the protection diodes and mixers,
- the digital section, with the averaging oscilloscope and the computer.

A stable frequency is provided by a synthesized oscillator whose sinusoidal output is divided into a reference signal and a “to sample” excitation signal. The spin-echo signal, phase sensitive detected in two orthogonal channels, is averaged in the digital oscilloscope and stored in the computer.

The spin-echo signal can be separated from the FID and spurious signals (including receiver recovery effects) following the “ $\pi/2$ - $\tau$ - $\pi$ - $\tau$ ” sequence by phase switching and, additionally, by an electronic transmit/receive switch, [Riedi 1994, Lord 1995]. The recovery time of the spectrometers is about 6  $\mu$ s, depending on the frequency range and some other experimental conditions.

## 5. Experimental results and discussion

In the thesis several systems of manganese perovskites are studied: “cubic” perovskites:

$\text{La}_{1-x}(\text{Sr,Ca})_x\text{MnO}_3$  synthesized by the ceramic method, nanoparticles of  $\text{La}_{0.75}\text{Sr}_{0.25}\text{MnO}_3$  prepared by the sol-gel method and bilayered perovskites:  $\text{La}_{2-2x}\text{Sr}_{1+2x}\text{Mn}_2\text{O}_7$  prepared either as single crystals by the floating zone technique and then powdered ( $0.3 \leq x \leq 0.5$ ) or synthesized originally as powder samples ( $0.5 \leq x < 1$ ) by the solid state reaction method.

### 5.1 $\text{La}_{0.875}\text{Sr}_{0.125}\text{MnO}_3$ and $\text{La}_{0.85}\text{Sr}_{0.15}\text{MnO}_3$ $^{55}\text{Mn}$ and $^{139}\text{La}$ NMR

In Fig. 3 the  $^{55}\text{Mn}$  frequency swept spectra measured at various temperatures ranging from 4.2 K to 225 K are shown. In all the presented NMR results at no applied magnetic field the measured signal comes mostly from domain walls owing to their larger enhancement factor. The dependences of the spin echo signal on the pulse length were measured at the maximum pulse amplitude for most of the resonance lines observed in the frequency swept spectra, starting from short pulses (mostly 0.1  $\mu$ s) to 1-2  $\mu$ s in order to find the first maximum of the echo signal, i.e. to determine the optimal excitation conditions. Unless stated differently, the presented frequency swept spectra are measured for excitation conditions which are optimal for the DE line. Usually, the enhancement factor of the  $\text{Mn}^{4+}$  line was found to be slightly larger and for the  $\text{Mn}^{3+}$  resonances - slightly smaller than for the DE line. A correction of the frequency response of the spectrometer was provided by inserting a 6 dB attenuator at the top of the probehead, which was found to reduce substantially the standing waves arising from a lack of impedance matching of the untuned coil. As the exact frequency response of the spectrometer and the frequency dependence of the enhancement factor were not known, the spectra are presented with no frequency correction.

At 4.2 K we observe several lines, namely  $\text{Mn}^{4+}$  line (at 327 MHz), the DE line (around 400 MHz) and two  $\text{Mn}^{3+}$  lines (ranging from 425-550 MHz). The appearance of several lines in the  $^{55}\text{Mn}$  spectra suggests the occurrence of phase separation in the compound

studied, in agreement with results of [Allodi 1997, Papavassiliou 1999, 2000, Renard 1999, Kapusta 2000a, 2000b, Novak (2004)]. The origin of the  $\text{Mn}^{4+}$  and  $\text{Mn}^{3+}$  lines are the Mn cations, which are in ferromagnetic insulating (FMI) regions, while the DE line is associated with Mn cations of intermediate valence, which is related to a fast, DE driven,  $3d e_g$  electron hopping between the  $\text{Mn}^{3+}$  and  $\text{Mn}^{4+}$  ions leading to ferromagnetism and metallicity (FMM) of these regions [Matsumoto 1970]. The ground state of the  $\text{La}_{0.875}\text{Sr}_{0.125}\text{MnO}_3$  compound in the literature [Dabrowski 1999] is reported to be FMI, however, at low temperatures we observe signals not only from FMI, but also from FMM regions. This indicates that there exists a phase separation into FMM and FMI regions in the compound studied. The size of the metallic-like regions in lightly doped manganites reported in the literature varies from 10 Å to 100 Å [Hennion 1998].

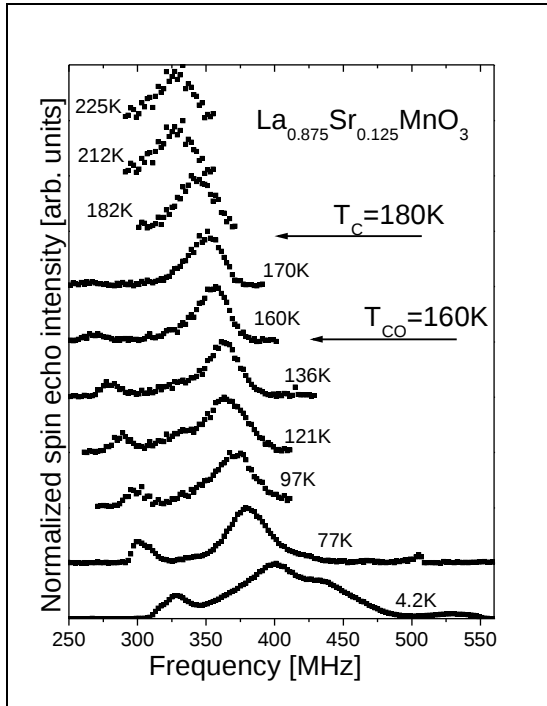


Fig. 3. The  $^{55}\text{Mn}$  frequency swept NMR spectra of  $\text{La}_{0.875}\text{Sr}_{0.125}\text{MnO}_3$  at various temperatures.  $T_{\text{CO}}$  and  $T_{\text{C}}$  are the charge ordering temperature and Curie temperature respectively, reported in the literature [Dagotto 2001].

As can be seen in Fig. 3, the DE line exists well above the bulk magnetic ordering temperature,  $T_{\text{C}}$  of 180 K and the signal was measured even at 225 K. This fact is attributed to long lived FMM regions (FM polarons [Salafranca 2006]). The fast diminishing of the  $\text{Mn}^{3+}$  signal with increasing temperature is due to a fast decrease of the spin-spin relaxation time,  $T_2$  and at 77 K very weak  $\text{Mn}^{3+}$  signals are observed at 420 MHz and at 500 MHz. A fast decrease of the  $\text{Mn}^{3+}$  signal from FMI regions with increasing temperature was also observed

in lightly Ca doped cubic manganese perovskite,  $\text{La}_{0.9}\text{Ca}_{0.1}\text{MnO}_3$  [Algarabel 2003]. The FMI  $\text{Mn}^{4+}$  line is observed up to 160 K, which is reported to be the temperature of transition to the charge ordered state [Dagotto 2001].

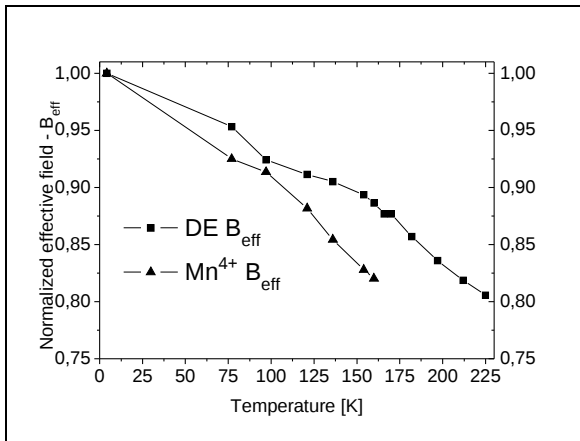


Fig. 4. Normalised effective field,  $B_{\text{eff}}$  versus temperature (for the FMI  $\text{Mn}^{4+}$  line and Mn ions in the DE regions of the  $\text{La}_{0.875}\text{Sr}_{0.125}\text{MnO}_3$  compound). Lines are guides for eyes only.

Normalised temperature dependences of the effective field at nucleus,  $B_{\text{eff}}$  of the  $\text{Mn}^{4+}$  and Mn cations in the DE regions are shown in Fig. 4. Points on the plot are central frequencies of Gaussian curves fits to the experimental data. At 4.2 K the  $B_{\text{eff}}$  at the  $\text{Mn}^{4+}$

nuclei in the FMI regions amounts to 31.26 T and at the Mn nuclei in FMM regions (averaged

Mn<sup>4+</sup> and Mn<sup>3+</sup> valence state) it is higher and amounts to 37.9 T (400 MHz). The decrease of the  $B_{eff}$  of both lines is due to a decrease of the manganese magnetic moment,  $\langle S_z \rangle$ , with temperature. For the DE line  $B_{eff}$  decreases merely by 17% between 4.2 K and 212 K. Since the  $B_{eff}$  is approximately proportional to the average spin magnetic moment, this indicates almost fully saturated Mn magnetisation in the FMM regions in this temperature range. The existence of the FMM regions above the  $T_C$  was observed by NMR also in other manganese perovskites [Kapusta 1999]. The respective change of the Mn<sup>4+</sup>  $B_{eff}$  is larger and amounts to 18%, between 4.2 K and 154 K, compared to 10.7% for the DE line at this temperature range. This indicates a weaker magnetic coupling in the FMI than in the FMM regions. A similar effect was found in the lightly Ca doped manganite system [Kapusta 2000]. Signals from the Mn<sup>3+</sup> ions at 4.2 K in the FMI regions range from 425 MHz (40.28 T) to 550 MHz (52.12 T). Such a broad distribution is due to the large anisotropy of the Mn<sup>3+</sup> hyperfine field. Mn<sup>3+</sup> is a Jahn-Teller ion and thus a different occupation of the  $e_g$  orbitals can be expected. Additionally, in the case of Mn<sup>3+</sup> ion the orbital moment is not quenched and can be of 0.05-0.1  $\mu_B$  (4-6% of the spin magnetic moment) in the lightly Sr doped cubic manganese perovskites [Koide 2001].

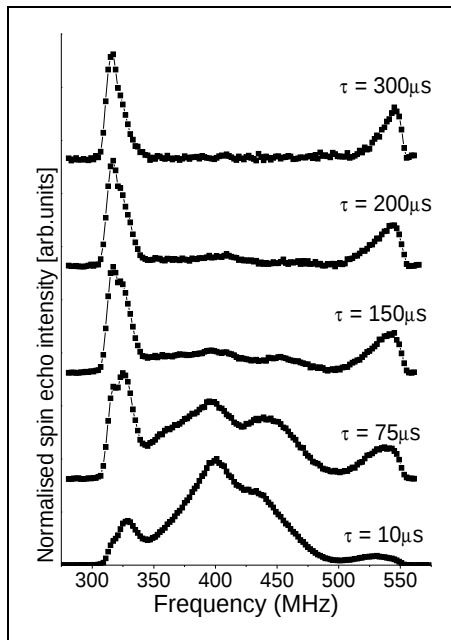


Fig. 5. <sup>55</sup>Mn NMR spin echo spectra of the La<sub>0.875</sub>Sr<sub>0.125</sub>MnO<sub>3</sub> compound at 4.2 K and different values of pulse spacing,  $\tau$ . Lines are guides for eyes only.

In order to identify the origin of the Mn<sup>3+</sup> lines at 440 MHz and at 530 MHz at 4.2 K, measurements with various pulse spacing,  $\tau$  were carried out. Their results for  $\tau$  ranging from 10  $\mu$ s to 300  $\mu$ s are presented in Fig. 5. As  $\tau$  increases, the intensity of the DE line decreases and the Mn<sup>4+</sup> and Mn<sup>3+</sup> lines at 325 MHz and 530 MHz, respectively, remain dominant. The Mn<sup>3+</sup> line at 530 MHz persists for higher pulse spacing, indicating that nuclei contributing to this signal have a longer spin-spin relaxation time  $T_2$  compared with nuclei contributing to the Mn<sup>3+</sup> line at 440 MHz. The line with shorter  $T_2$  (at lower frequency) is attributed to the domain wall centre and the line which has a longer  $T_2$  (at higher frequency) is attributed to the domain wall edge, where the ionic magnetic moments are within or close to the easy magnetisation direction (EMD) [Weisman 1973, Davis 1976, Leung 1977]. The signal from domain wall centre corresponds to the ions with magnetic moments along (or close to) the hard magnetisation direction(s) (HMD). However, according to this line attribution, the line at 440 MHz attributed to domain wall centre should differ in enhancement factor, which is not the case. The enhancement factor of the line at 440 MHz is found to be almost the same as for the line at 530 MHz.

Additionally, measurement at 3 T and at 3.2 K was carried out to verify the attribution of Mn<sup>3+</sup> lines described above (Fig. 6). As it can be seen at 3 T the FMI Mn<sup>4+</sup> and FMM DE lines shift towards lower frequencies, as the Mn<sup>3+</sup> line at 530 MHz also does. However, the Mn<sup>3+</sup> line at 440 MHz does not shift, but only decreases in intensity compared with other lines. The shift towards lower frequencies confirms that the observed signals, from the Mn<sup>4+</sup>

ions and from regions where the DE interaction is effective, come from FM ordered regions. The hyperfine field,  $B_{HF}$  which is the dominant component of the  $B_{eff}$ , is negative (i.e. antiparallel to the electronic spin moment,  $\mu_s$  and to the applied field,  $B_0$ ). Therefore with increasing applied field the  $B_{eff}$  and the corresponding resonant frequency decrease. Resonant frequencies decrease by 28 MHz and 18 MHz for the  $Mn^{4+}$  line and the DE line, respectively. A smaller change in the case of the DE line is probably due to a higher demagnetising field and/or magnetocrystalline anisotropy in the DE regions.

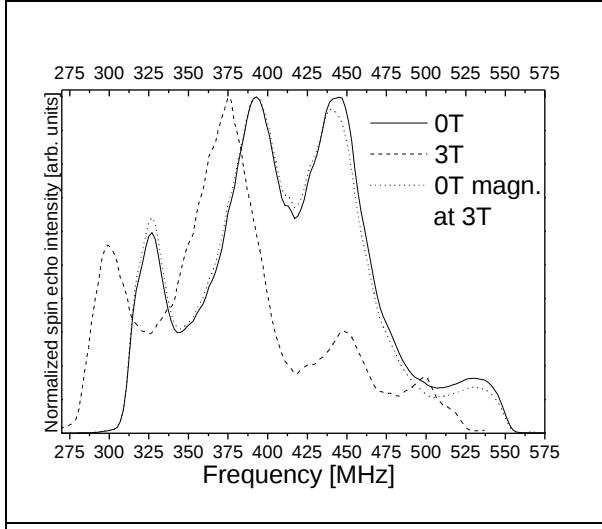


Fig. 6.  $^{55}Mn$  NMR spin echo spectra of the  $La_{0.875}Sr_{0.125}MnO_3$  compound at 3.2 K at no applied field (solid line), at 3 T (dashed line) and at 0 T after switching the field off (dotted line).

In the case of  $Mn^{3+}$  lines, assuming that observed signals come from domain walls, which is usual in NMR experiments due to higher enhancement factor of nuclei in domain walls than within domains, the shift of the line at 530 MHz means that magnetic moments of ions contributing to this line are

parallel to the applied field. This means that they may be located in domain wall edges. In domain wall centres magnetic moments can be perpendicular to the applied field. Since the  $B_{eff}$  is much larger than the applied field (42 T compared to 3 T) no shift of the line at 440 MHz is observed at 3 T.

The situation is in fact more complicated, because in the compound studied there are two non equivalent Mn sites. Taking into account only crystallographic structure there is only one Mn site, but introducing magnetic order, the relative distortions and tilting of manganese-oxygen octahedra results in two non equivalent Mn sites. For these two sites angles between direction of the magnetic moment and main directions in the octahedron are different. The presence of two non equivalent Mn sites can be the reason of the asymmetric line shape of the  $Mn^{4+}$  FMI line at 330 MHz (see Fig. 5). However, the observed  $Mn^{3+}$  lines cannot be due to two non equivalent Mn sites, because they both should shift towards lower frequencies at the applied field, which is not observed for the line at 440 MHz.

An alternative explanation for the lack of the shift in the applied field could be its origin in AF coupled moments. However, as was mentioned, the enhancement factor,  $\eta$  is similar for both lines while it should be much smaller for the signal from AF coupled moments than for FM coupled [Turov 1970].

With increasing content of Sr (hole doping) the average ionic radius of the perovskite A-site cations increases (the ionic radius of  $Sr^{2+}$  is larger than  $La^{3+}$ ). This is called the chemical pressure effect [Xu 2003], which results in the increase of the Mn-O-Mn bond angle and a decrease of the distortions [Xiong 1999]. Therefore, one might expect a higher effectiveness of the DE interaction (effectiveness of the DE interaction increases with increase of the Mn-O-Mn bond angle). The FMM phase content should also increase with increasing Sr doping, thus it should be higher in the  $x=0.15$  Sr doped compound than in the compound with  $x=0.125$ . As expected, we observe this kind of behaviour in the NMR spectra.

The  $^{55}\text{Mn}$  NMR frequency swept spectra of the  $\text{La}_{0.85}\text{Sr}_{0.15}\text{MnO}_3$  compound at different pulse spacing,  $\tau$  and at 4.2 K are presented in Fig. 7. Similarly to  $\text{La}_{0.875}\text{Sr}_{0.125}\text{MnO}_3$ , the spectra of  $\text{La}_{0.85}\text{Sr}_{0.15}\text{MnO}_3$  at 4.2 K reveal the co-existence of FMI and FMM regions. The line at 334 MHz is due to  $\text{Mn}^{4+}$  ions and signals ranging from 410 to 550 MHz are due to  $\text{Mn}^{3+}$  ions in the FMI regions while the line at 396 MHz is due to FMM regions.

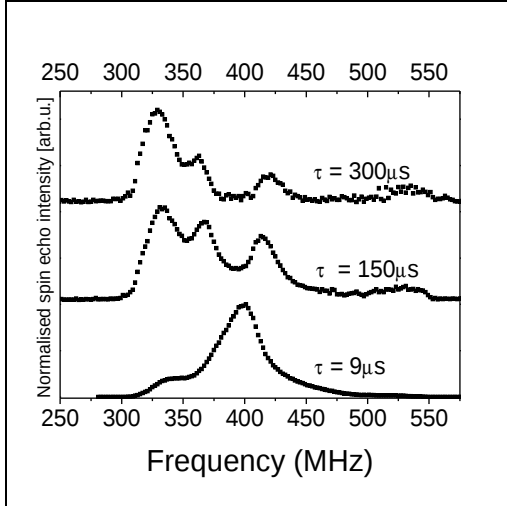


Fig. 7.  $^{55}\text{Mn}$  NMR spin echo spectra of the  $\text{La}_{0.85}\text{Sr}_{0.15}\text{MnO}_3$  compound at 4.2 K with three different values of the pulse spacing,  $\tau$ .

In Fig. 7 it is clearly visible that a dip in the centre of the DE line appears with increasing pulse spacing. The effect can be explained by the Suhl-Nakamura (S-N) interaction [Suhl 1958, Nakamura 1958, Davis 1974] between nuclear spins of neighbouring Mn ions. The nuclear spin, which sees the electronic spin of its own ion through the hyperfine coupling, excites a spin wave through this coupling, and another nuclear spin absorbs it through its hyperfine coupling [Suhl 1958]. The observed dependence of the spectra on the pulse spacing means that nuclear spins, which precess at or near the central frequency, reveal a faster spin-spin relaxation than spins contributing to the wings of the resonance line. As the centre of the DE resonance line originates mainly from the spins inside the DE regions, a minimum at the line centre denotes that the neighbouring manganese ions are magnetically equivalent, which makes the S-N interaction effective. This is much less effective at the boundaries of DE regions where Mn neighbours differ in terms of magnetic moments and/or their directions, which prevents the exchange of virtual spin waves and results in a slower spin-spin relaxation. An indication of the S-N interaction is the frequency dependence of  $T_2$  which should have a minimum at the centre of the DE line. Such a minimum is observed in the case of  $\text{La}_{0.85}\text{Sr}_{0.15}\text{MnO}_3$ , but not for  $\text{La}_{0.875}\text{Sr}_{0.125}\text{MnO}_3$  (see Fig. 8).

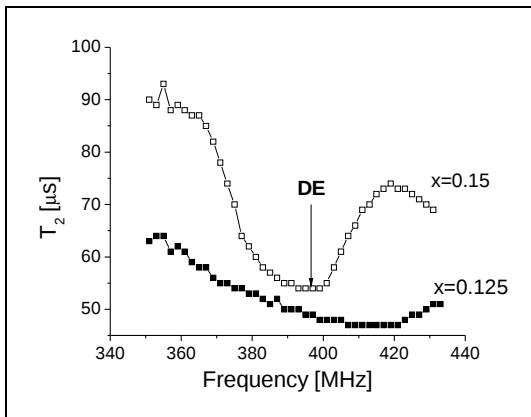


Fig. 8. Frequency dependence of the spin-spin relaxation time,  $T_2$  for  $x=0.125$  and  $x=0.15$  compounds. The DE mark denotes the resonant frequency. Lines are guides for eyes only.

For the  $\text{La}_{0.875}\text{Sr}_{0.125}\text{MnO}_3$  compound the DE line vanishes with increasing pulse spacing and no dip at the line centre appears (Fig. 5). The S-N interaction was also observed in other ferromagnetic metallic manganites [Savosta 2001, Rybicki 2004]. On this basis we conclude that the S-N interaction is effective only in the  $x=0.15$  doped compound and that the regions, where the DE interaction is dominant are much larger in size in the  $x=0.15$  than in the  $x=0.125$  doped compound. The FMM clusters of the size of 10 nm were also found in the  $x=0.15$  compound by the small angle neutron scattering (SANS) technique [Ibarra et al., unpublished].

In manganese perovskites, besides  $^{55}\text{Mn}$  NMR also signals from  $^{139}\text{La}$  nuclei have been measured in several compounds doped with calcium [Allodi 1997, Papavassiliou 1997, 2001] or with sodium [Savosta 1999]. Lanthanum nucleus (nuclear spin  $I=7/2$ ) is subjected to the transferred hyperfine field (from manganese neighbours) and dipolar interactions with electronic moments as well as to the quadrupolar coupling with the electric field gradient. However, satellite lines which would indicate the presence of quadrupolar interactions have never been observed experimentally in manganese perovskites. The hyperfine field originates indirectly from the overlap of the Mn  $|3d\rangle$  with oxygen  $|2p\rangle$  wave functions, in conjunction with  $\sigma$  bonding of the oxygen with  $|sp^3\rangle$  hybrid states of the  $\text{La}^{3+}$  cation [Papavassiliou 1997].

The frequency swept spectra of  $^{139}\text{La}$  NMR are presented in Fig. 9. For both compounds with different Sr doping two lines are observed, however with different relative intensities. Resonant frequencies are obtained by fitting Gaussian curves to the data and they amount to  $17.64\pm 0.09$  MHz and  $32.80\pm 0.11$  MHz for  $x=0.125$  Sr doped compound. For  $x=0.15$  Sr doping resonant frequencies amount to  $18.57\pm 0.04$  MHz and  $32.92\pm 0.14$  MHz. The corresponding values of the  $B_{\text{eff}}$  at the  $^{139}\text{La}$  nuclei amount to 2.94 T and 5.46 T for the  $x=0.125$  compound and 3.09 T and 5.48 T for the  $x=0.15$  one. The difference between effective fields of those two lines for both compounds is close to 2.5 T and it cannot be explained by the anisotropy of the dipolar field,  $B_D$  which is of order of a few tenths of Tesla.

The  $^{139}\text{La}$  signal at frequency 20 MHz and a tail at higher frequencies (up to 35 MHz) were observed also for  $\text{La}_{0.875}\text{Ca}_{0.125}\text{MnO}_3$  compound [Papavassiliou 2001]. The authors suggested that the higher frequency signal is due to the formation of Mn octant cells with enhanced Mn-O wave functions overlap resulting in a higher effective field on  $^{139}\text{La}$  nuclei. The signal at higher frequency is not observed for the FMM manganese perovskites doped both with Sr (see the spectrum for  $x=0.3$  Sr doped compound, Fig 4.9) and with Ca [Papavassiliou 1998], where a single line at the lower frequency is observed only. Therefore, one can assume that the line at lower frequency is due to  $^{139}\text{La}$  ions in FMM regions and the higher frequency line is due to  $^{139}\text{La}$  in charge localised (CL) FMI regions. This assumption can be supported by the fact that the relative intensity of the CL line is higher for  $x=0.125$  doped compound, thus meaning that the amount of the FMI phase is higher for this compound than for the  $x=0.15$  one.

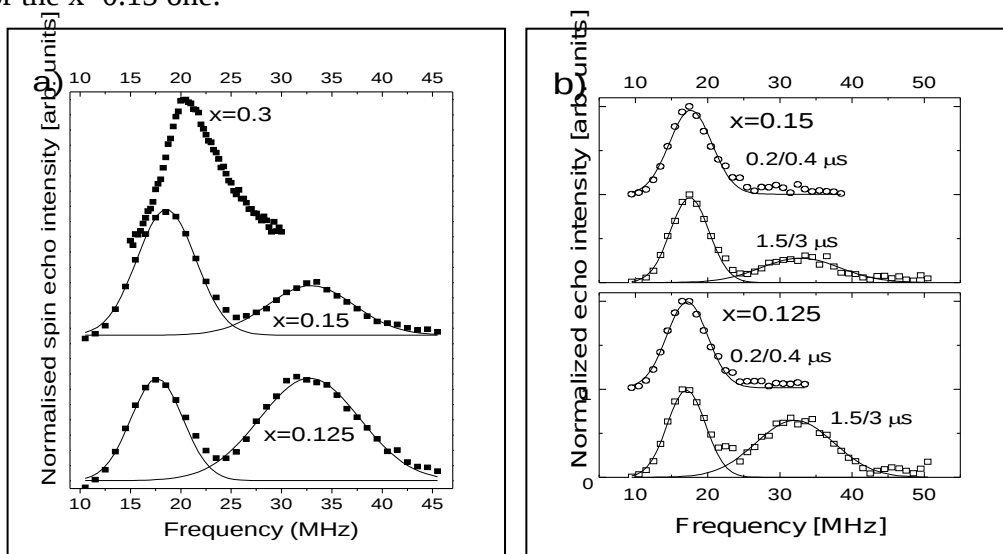


Fig. 9. a)  $^{139}\text{La}$  NMR frequency swept spectra at 4.2 K, for  $x=0.125$ ,  $x=0.15$  Sr doped compounds and for  $x=0.3$ ; b) together with the spectra measured with shorter exciting pulses

for both compounds. The solid curves are Gaussian fits to the experimental data.

As can be seen in Fig. 9b the line at lower frequency requires a smaller radio frequency (rf) pulse amplitude or pulse length, whereas the line at higher frequency is not observed for a small pulse length (0.2  $\mu$ s). This indicates that the enhancement factor,  $\eta$  of nuclei contributing to the signal at lower frequency is bigger. A possibility that one of observed lines could be due to some remaining AF phase (the AF – FM phase boundary occurs for 10% of Sr doping) can be excluded, since the  $^{139}\text{La}$  signal from AF phase can only be observed at high applied fields. Such a signal was observed at 7 T in the antiferromagnetic  $\text{La}_{0.5}\text{Ca}_{0.5}\text{MnO}_3$  [Allodi 1998] and at similar fields in  $\text{La}_{0.95}\text{Sr}_{0.05}\text{MnO}_3$  [Kumagai 1999]. Even if  $^{139}\text{La}$  signal from the AF phase could be observed at 0 Tesla, it should correspond to much lower frequencies than the signal from the FM phase, Since the hyperfine transferred field from AF ordered manganese neighbours of La would be smaller than from FM ordered Mn ions. So this hypothetical La signal from AF phase at lower frequencies should, according to previous studies [Allodi 1998, Kumagai 1999, Yakubowskii 2000], have a smaller enhancement factor and shorter relaxation times, which is not the case (see Fig. 9b). Both the spin-spin and spin-lattice relaxation times are found to be more than two times bigger for the line at lower frequency.

## 5.2 Nanoparticles of $\text{La}_{0.75}\text{Sr}_{0.25}\text{MnO}_3$

Fig. 10 presents  $^{55}\text{Mn}$  NMR spin echo spectra at zero field, at 0.2 T and at 0.5 T for samples with grains of micrometric size (SM) and with average grain size of 114 nm (S114) and 33 nm (S33). The dominant DE line centred close to 380 MHz and a weak signal at lower frequencies (315-340 MHz) ascribed to  $\text{Mn}^{4+}$  ions in FMI regions located in the outer layers of the grains are observed. Our observation of two resonant lines is similar to that in the NMR  $^{55}\text{Mn}$  study of  $\text{La}_{0.66}\text{Ca}_{0.33}\text{MnO}_3$  nanoparticle materials [Bibes 2003, Savosta 2004]. Similarly to the results presented there the intensity of the signal at 315-340 MHz per unit mass decreases with increase of the average grain size (Fig. 11). The relative amount of the FMI phase estimated from the line intensities of the spectra at zero field is of 3% and 1% for the samples S33 and S114, respectively.

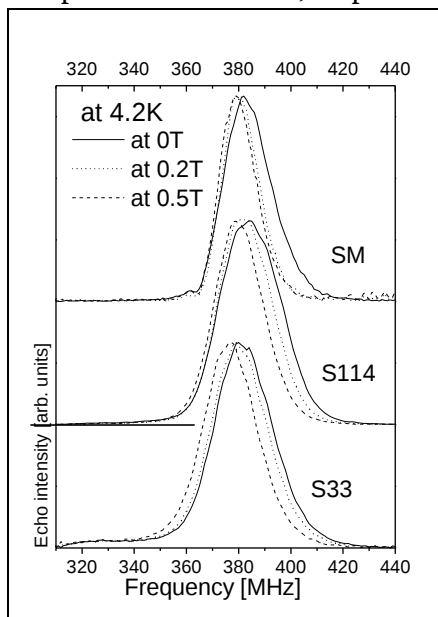


Fig. 10. Normalised NMR  $^{55}\text{Mn}$  spin echo spectra of  $\text{La}_{0.75}\text{Sr}_{0.25}\text{MnO}_3$  (SM, S114 S33 samples) at 4.2 K, at 0 T (solid lines), 0.2 T (dotted lines) and 0.5 T (dashed lines).

The values of the resonant frequencies of the DE line obtained from Gaussian curve fits to the spectra for samples S114, S33 and SM at 0 T are 384.5 MHz, 381.9 MHz and 383.4 MHz respectively. Since the magnitude of the hyperfine field,  $B_{\text{HF}}$  is approximately proportional to the average electronic spin moment ( $\langle S \rangle$ ),  $\vec{B}_{\text{HF}} = \hat{A} \langle S \rangle$ , where  $\hat{A}$  is the hyperfine coupling tensor, therefore different values of the  $B_{\text{HF}}$  for all samples could be attributed to a slightly different  $\text{Mn}^{3+}/\text{Mn}^{4+}$  ratio in all studied samples. This may be due to a possibly different

oxygen stoichiometry in different samples resulting in non stoichiometric  $\text{Mn}^{3+}/\text{Mn}^{4+}$  ratio and/or an influence of the related negative pressure in small grains, which would decrease the value of  $B_{HF}$  [Kapusta 2001].

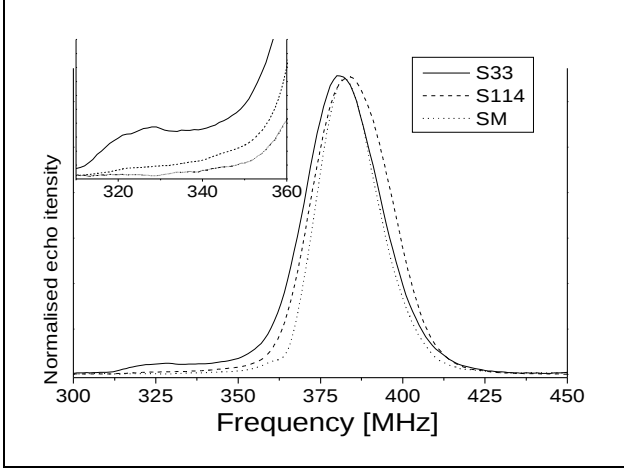


Fig. 11. Normalized  $^{55}\text{Mn}$  spin echo spectra of  $\text{La}_{0.75}\text{Sr}_{0.25}\text{MnO}_3$  of SM (dashed line), S114 (dotted line) S33 (solid line) samples at 4.2 K and at 0 T. Zoomed view of low frequency region is presented in the inset.

The DE line shifts towards lower frequencies with increasing applied field as expected for the hyperfine field antiparallel to the Mn magnetic moment. For the sample S114 at 0.5 T, the  $B_{eff}$  is reduced to 36.02 T from 36.45 T at no applied field, for the sample S33 it decreases from 36.20 T to 35.72 T and for the SM sample from 36.34 T to 35.98 T. One can conclude that the demagnetizing field,  $B_{dem}$  is smaller than 0.2 T and that even at the smallest applied magnetic field our samples are the most likely in a single domain state.

However, the spin-spin relaxation time ( $T_2$ ) for all studied samples reveals a non-exponential behaviour at 0 T, whereas  $T_2$  decreases with a single exponential manner at 0.5 T (Fig. 12). This indicates the presence of some domain wall-like magnetic inhomogeneities in all the studied samples at 0 T, which disappear after applying magnetic field of 0.5 T. Similar behaviour was also observed by Savosta et al. [Savosta 2004]. On this basis we assume that the DE line originates from Mn ions located both in domains and domain-wall like inhomogeneities (i.e. close to surface regions, where magnetic moments change their orientation similarly to the behaviour of magnetic moments in domain walls). The existence of typical domain walls is put in question due to very small size of grains in the samples S33 and S114. A similar assumption was also made in [Savosta 2004]. The nuclei in domain walls have shorter spin-spin relaxation time than nuclei in domain interiors [Weisman 1973, Davies 1976, Leung 1977].

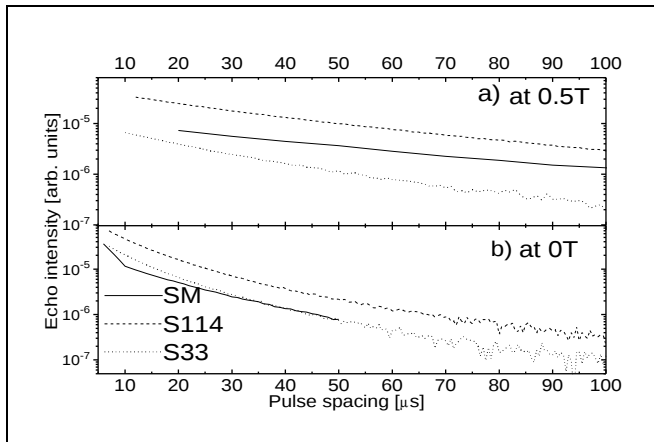


Fig. 12. Spin echo decay curves for resonant frequencies of the DE lines at 4.2 K for all studied samples of the  $\text{La}_{0.75}\text{Sr}_{0.25}\text{MnO}_3$ ; a) at 0.5 T and b) at 0 T. Note the logarithmic scale of the echo intensity.

Due to presence of signals both from domains ( $T_2^D$ ) and from domain walls (or domain wall like regions) ( $T_2^{DW}$ ), two exponents have to

be used in order to fit the decay curve of the spin-echo signal. The experimental data were fitted

$$A(\tau) = A_{\tau=0}^D \exp\left(-\frac{2\tau}{T_2^D}\right) + A_{\tau=0}^{DW} \exp\left(-\frac{2\tau}{T_2^{DW}}\right) \quad (1)$$

where  $A(\tau)$  and  $A_{\tau=0}^{D,DW}$  are the spin-echo amplitudes at the time  $\tau$ , and  $\tau=0$  (for domains and domain walls (or domain wall-like regions), respectively). The obtained values of the spin-spin relaxation times for nuclear magnetic moments,  $T_2^D$  and  $T_2^{DW}$  for all the samples at 0 T, at 4.2 K and 77 K are presented in table 1.

Sample	4.2 K		77 K	
	$T_2^{DW}$ [ $\mu$ s]	$T_2^D$ [ $\mu$ s]	$T_2^{DW}$ [ $\mu$ s]	$T_2^D$ [ $\mu$ s]
SM	$4.3 \pm 0.2$	$31.8 \pm 1.2$	$11.1 \pm 0.2$	$35.6 \pm 0.6$
S114	$12.1 \pm 0.1$	$38.7 \pm 0.6$	$9.2 \pm 1.2$	$24.4 \pm 4.7$
S33	$10.7 \pm 0.1$	$33.3 \pm 0.5$	$7.6 \pm 1.5$	$22.5 \pm 6.6$

Table 1. Spin-spin relaxation times for nuclear magnetic moments in domains ( $T_2^D$ ) and in domain walls (or in domain wall like regions) ( $T_2^{DW}$ ), obtained using equation 1 for all the studied samples of  $\text{La}_{0.75}\text{Sr}_{0.25}\text{MnO}_3$  at 0 T, 4.2 K and 77 K measured at the resonant line maximum for each sample.

Also for all the three samples of  $\text{La}_{0.75}\text{Sr}_{0.25}\text{MnO}_3$  the frequency swept spectra at 0 T and at 0.5 T for various pulse spacing,  $\tau$  were measured. With increasing pulse spacing a dip at the centre of the DE line similar to that observed for the case of  $\text{La}_{0.85}\text{Sr}_{0.15}\text{MnO}_3$  compound is observed, which is due to the S-N interaction. Also the frequency dependence of  $T_2$  has a minimum at the central frequency (Fig. 13). The values of the  $T_2$  were calculated from all measured frequency swept spectra with different pulse spacing used. They were obtained assuming a single exponential decay of the spin-echo signal (see Fig 12a) i.e. a single domain state of samples at 0.5 T. The Suhl-Nakamura interaction for  $^{55}\text{Mn}$  ion in bulk metallic  $\text{La}_{0.7}\text{Ca}_{0.3}\text{MnO}_3$  compound has the effective range of 35 Å at 140 K [Savosta 2001].

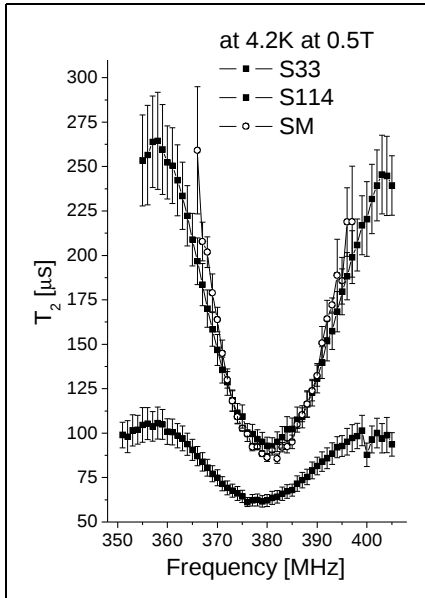


Fig. 13. Frequency dependence of the spin-spin relaxation time,  $T_2$  for samples S33, S114 and SM of  $\text{La}_{0.75}\text{Sr}_{0.25}\text{MnO}_3$  at 4.2 K and at 0.5 T with error bars marked.

As can be seen in Fig. 13, samples S114 and SM have similar values of the  $T_2$ , for a given frequency, while  $T_2$  of the S33 sample is significantly smaller. This means that the relaxation of nuclear spins is faster. In the metallic-like perovskite manganites there are two main mechanisms responsible for the spin-spin relaxation of nuclear magnetic moments [Savosta 2004]. The first one are fluctuations of the hyperfine fields caused by hopping of electron holes,  $T_2(\text{hop})$ . The second mechanism is the spin-spin relaxation due to the S-N interaction,  $T_2(\text{SN})$ , which is not effective at the sides of the resonant line, where the mechanism due to electron (hole) hopping has to be considered only. Therefore, both relaxation processes can be separated using the formula

[Savosta 2004]:

$$T_2^{-1} = T_2^{-1}(hop) + T_2^{-1}(SN) \quad (2)$$

where  $T_2^{-1}$  is the value for given frequency, taken from Fig. 13. From this formula the contribution of the S-N interaction to the relaxation rate is derived. The values of the relaxation rates,  $T_2^{-1}(SN)$  amount to  $6.97 \text{ ms}^{-1}$ ,  $6.61 \text{ ms}^{-1}$  and  $7.63 \text{ ms}^{-1}$  for S33, S114, SM samples respectively for the DE line and one can conclude that in all the samples studied the effective range of the Suhl-Nakamura interaction is comparable or smaller than the size of DE regions.

Nanosized samples exhibit smaller Suhl-Nakamura contribution to the relaxation rate than the sample with micrometric grains. This can be explained knowing that the effectiveness of the S-N interaction depends on the number of nuclear spins, which precess at or near the resonance frequency and this number can be smaller in samples with nanometric grains. The obtained results of the DE line widths (given as full widths at half maximum) from the Gaussian curve fits support this finding. The DE line of the S33 sample is the broadest (the broader the resonance line - the less nuclear spins, which precess at or near the resonance frequency). Similar observation was made for the nanoparticles of  $\text{La}_{0.7}\text{Sr}_{0.3}\text{MnO}_3$  [Savosta 2004]. The  $T_2^{-1}(hop)$  is larger for S33, i.e. for sample with smallest grains ( $T_2^{-1}(hop) \cong 1/100 \mu\text{s}^{-1}$ ) than for samples S114 and SM ( $T_2^{-1}(hop) \cong 1/260 \mu\text{s}^{-1}$ ). This implies, that in the sample with the smallest grains electrons and holes are moving slower, since  $T_2^{-1} \sim \tau_{hop}$  [Savosta 2004], where  $\tau_{hop}$  is the correlation time of electron (hole) hopping [Savosta 1999].

One can also notice that nuclear spin-spin relaxation times,  $T_2$  of Mn measured at 0.5 T are considerably longer than those obtained at 0 T. The  $T_2$  at 0 T lies in the range 25-30  $\mu\text{s}$  for all samples (table 1) while at 0.5 T it amounts to 62  $\mu\text{s}$ , 93  $\mu\text{s}$  and 86  $\mu\text{s}$  for S33, S114 and SM samples respectively. This fact is a result of the two factors. First, the contribution to the spin-spin relaxation time from nuclei within domain walls (or domain wall like regions) decreases and is later eliminated as domain walls (domain wall like regions) are removed by the applied field [Leung 1977]. As was shown  $T_2$  for nuclei within domain walls is shorter than for nuclei in domains. The second factor is the fact that the S-N interaction depends on the external field, so that  $T_2$  increases as the external field increases [Hone 1969, Davis 1974]. This effect was observed in the manganese ferrite [Davis 1976] and in  $\text{La}_{0.69}\text{Pb}_{0.31}\text{MnO}_3$  [Leung 1977].

## 5.2 Bilayered manganese perovskites, $\text{La}_{2-2x}\text{Sr}_{1+2x}\text{Mn}_2\text{O}_7$

Before presenting the NMR results a closer look is given at the contribution to the hyperfine field,  $\vec{B}_{HF}$  called spin-dipolar field,  $\vec{B}_{S-d}$ , which is due to spins of electrons at individual orbitals and is given by the formula:

$$\vec{B}_{S-d} = g_s \mu_B \mu_0 \sum_i \left\{ \frac{\vec{s}_i r^2 - 3(\vec{s}_i \circ \vec{r}_0) \vec{r}_0}{r^5} \right\} \quad (3)$$

where  $g_s=2.0023$ ,  $\vec{s}_i$  is the spin of  $i$ th electron and  $\vec{r}_0$  is a unit vector along the leading vector,  $r$ . This field can be computed by multiplying the above equation by the electron density,  $\rho = \Psi_e^* \Psi_e$  and integrating over the electron coordinates [Abragam 1970]. In the compounds studied the  $\text{Mn}^{3+}$  ion has four electrons in the  $3d$  band in a high spin state, i.e. 3 electrons with spin up on  $t_{2g}$  orbitals and one electron with spin up on one of the two  $e_g$  orbitals. Calculations

of the spin-dipolar field,  $\vec{B}_{S-d}$  at nucleus produced by a single electron occupying one of the  $3d e_g$  orbitals were carried out in the Mathematica program using numerical integration. The results of calculations are presented in table 2.

$\vec{\mu}_s$ direction	$\vec{B}_{S-d}$ for $e_g$ orbital	
	$x^2 - y^2$	$3z^2 - r^2$
[100]	10,34T	-10,34T
[001]	-20,68T	20,68T

Table 2. Calculated values of the spin dipolar hyperfine field  $\vec{B}_{S-d}$  at Mn nucleus produced by a single electron occupying one of the  $3d e_g$  orbitals. The sign of the  $\vec{B}_{S-d}$  is taken with respect to the direction  $[xyz]$  of the spin moment,  $\vec{\mu}_s$ .

The frequency swept spectra of  $\text{La}_{1.4}\text{Sr}_{1.6}\text{Mn}_2\text{O}_7$  ( $x=0.3$ ) presented in Fig. 14 show that the DE line reveals a minimum at its centre with increasing pulse spacing. This is related to the frequency dependence of the spin-spin relaxation time  $T_2$  which reveals a minimum at the centre of the DE line. These two features result from the S-N interaction and were already described in details.

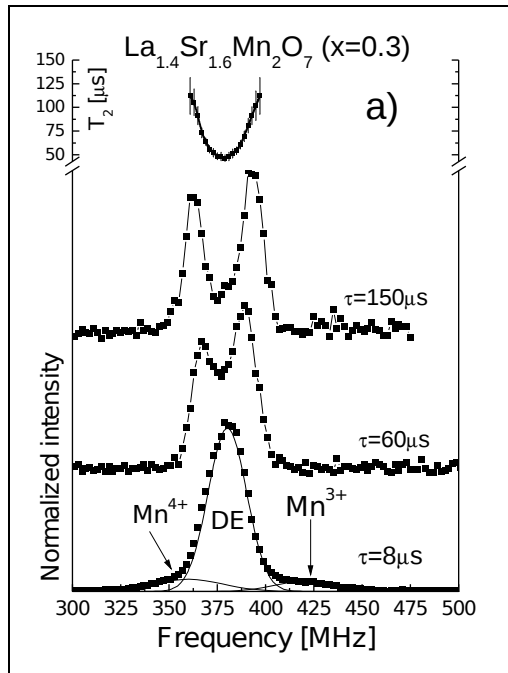


Fig. 14.  $^{55}\text{Mn}$  NMR spin echo spectra at 4.2 K at no applied field of  $\text{La}_{1.4}\text{Sr}_{1.6}\text{Mn}_2\text{O}_7$  ( $x=0.3$ ) for different pulse spacing. The solid lines at the bottom spectrum are Gaussian fits and the other lines are guides for eyes only. The upper plot presents the frequency dependence of the spin-spin relaxation time with error bars marked.

The occurrence of a dip at the centre of the DE line is not observed for  $\text{LaSr}_2\text{Mn}_2\text{O}_7$ , i.e.  $x=0.5$  (Fig. 15b) and there is no minimum in the frequency dependence of the  $T_2$  at the central frequency. On this basis we can conclude that the S-N interaction is not effective in the  $x=0.5$  doped compound and that the size of the DE regions is smaller than the effective radius of the S-N interaction in this compound, which can be due to AF ordering within the bilayer in this compound [Mitchell 2001]. On the contrary, the size of the DE regions is much larger than the effective radius of the S-N interaction in the  $x=0.3$  compound. This means that the DE regions in the  $x=0.5$  compound are of a nanometer in size, whereas they are at least tens of nanometers in the  $x=0.3$  compound. The strongest signal from the DE regions observed in the  $x=0.3$  compound can be due to its  $\text{Mn}^{3+}/\text{Mn}^{4+}$  ratio more preferable for DE interaction, but it can also be related to the fact that in this compound magnetic moments are perpendicular to the bilayer plane, while in the region  $0.33 \leq x \leq 0.5$  magnetic moments lie in the bilayer plane. This can correspond to different magnetocrystalline anisotropy and/or to a difference of the DE integral.

For the compounds with  $x=0.4$  and  $0.5$  one can notice that the DE line shifts towards higher frequencies at the larger pulse spacing, which can be attributed to the anisotropy of the effective field. Interestingly, for the  $x=0.3$  compound such a behaviour is not observed,

suggesting an isotropic effective field.

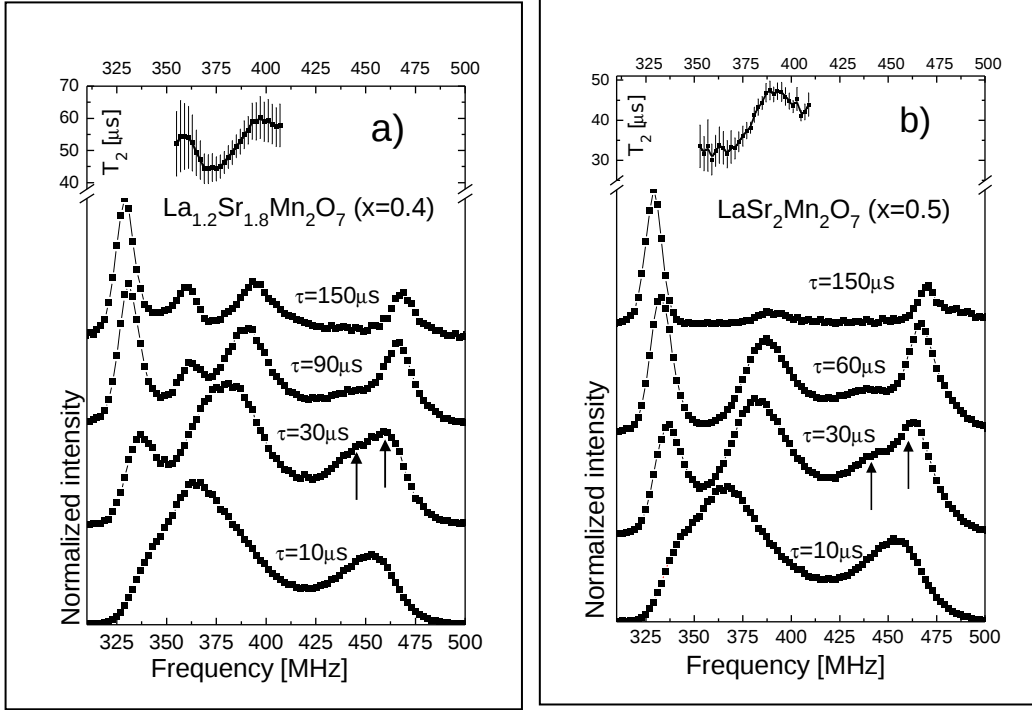


Fig. 15.  $^{55}\text{Mn}$  NMR spin echo spectra at 4.2 K and no applied field a) of  $\text{La}_{1.2}\text{Sr}_{1.8}\text{Mn}_2\text{O}_7$  ( $x=0.4$ ) for different pulse spacing and b) of  $\text{LaSr}_2\text{Mn}_2\text{O}_7$  ( $x=0.5$ ). Arrows on the spectra of both compounds for  $\tau=30\ \mu\text{s}$  indicate positions of the  $\text{Mn}^{3+}$  lines. The upper plot presents frequency dependence of  $T_2$  with error bars marked. Solid lines are guides for eyes only.

The effective magnetic field at nucleus,  $\vec{B}_{\text{eff}}$  i.e. the total magnetic field experienced by the nuclei of a “magnetic” ion at zero external magnetic field is a sum of the hyperfine field,  $\vec{B}_{\text{HF}}$  resulting mainly from the spin and orbital moments of the electron within the ion radius and the “local” field,  $\vec{B}_{\text{loc}}$ . The local field includes the classical dipolar field ( $\vec{B}_D$ ) resulting from other magnetic moments in the sample, the demagnetising field,  $\vec{B}_{\text{dem}}$  related to the macroscopic shape of the sample and the Lorenz field  $\vec{B}_{\text{Lor}}$ . The  $\vec{B}_{\text{HF}}$  can be written as a following sum:

$$\vec{B}_{\text{HF}} = \vec{B}_{\text{Fermi}} + \vec{B}_{\text{S-d}} + \vec{B}_{\text{orb}} + \vec{B}_T \quad (4)$$

where  $\vec{B}_{\text{Fermi}}$  is the Fermi contact field,  $\vec{B}_{\text{S-d}}$  and  $\vec{B}_{\text{orb}}$  are contributions from the spin dipolar interaction between the nucleus and the electronic spin and from the interaction between the nucleus and unquenched orbital moment of the electron respectively. The last element is the transferred hyperfine field, i.e. field produced by magnetic neighbours ( $\vec{B}_T$ ). The anisotropic terms of the total magnetic field experienced by the nuclei are:  $\vec{B}_{\text{S-d}}$ ,  $\vec{B}_{\text{orb}}$ ,  $\vec{B}_D$  and  $\vec{B}_T$ .

The spectra of the  $x=0.4$  and  $x=0.5$  compounds at short pulse spacing (Fig. 15), show two  $\text{Mn}^{3+}$  lines. With increasing pulse spacing the  $\text{Mn}^{3+}$  line at the lower frequency disappears and the one at the higher frequency stays at the longest pulse spacing used. The line which has a shorter  $T_2$  (lower frequency) is attributed to the domain wall centre and the line which has a longer  $T_2$  (higher frequency) is attributed to the domain wall edge, where the ionic magnetic moments are within or close to the easy magnetisation direction (EMD) [Weisman 1973, Davis 1976, Leung 1977]. The signal from domain wall centre corresponds to the ions with magnetic moments along (or close to) the hard magnetisation direction(s) (HMD).

As the  $x=0.3$  compound has the EMD along the  $c$  axis and with increasing doping the easy axis changes to the easy plane (i.e. to the  $ab$  plane), the variation of resonant frequencies can be attributed to the change in the EMD. Therefore we can conclude that the  $\text{Mn}^{3+}$  line at the lower frequency comes from ions which have their magnetic moments along the  $c$  axis and the line at the higher frequency results from ions, which have their magnetic moments within the  $ab$  plane.

Let us denote  $\vec{B}_{eff}^1$  and  $\vec{B}_{eff}^2$  as the effective fields corresponding to the lower and the upper resonance line, respectively. Using the equation 4 for the hyperfine field,  $\vec{B}_{HF}$ , one can write the following vector sums:

$$\vec{B}_{eff}^1 = \vec{B}_{Fermi} + \vec{B}_T + \vec{B}_D + \vec{B}_{orb} + \vec{B}_{s-d}^{[001]} \quad \text{and} \quad (5)$$

$$\vec{B}_{eff}^2 = \vec{B}_{Fermi} + \vec{B}_T + \vec{B}_D + \vec{B}_{orb} + \vec{B}_{s-d}^{[100]}, \quad (6)$$

where the superscript in the  $\vec{B}_{s-d}$  indicates the spin dipolar field produced by electrons of  $\text{Mn}^{3+}$  ions with magnetic moments along the  $c$  axis ([001]) or within the  $ab$  plane ([100]).

One can group contributions to effective fields  $\vec{B}_{eff}^1$  and  $\vec{B}_{eff}^2$  into isotropic and anisotropic parts. The isotropic part is  $\vec{B}_{Fermi}$ , which can be estimated for  $\text{Mn}^{3+}$  knowing that for manganese it is proportional to the spin moment of the parent ion at  $-10 \text{ T}/\mu_B$  [Asano 1987]. With 4 electrons on the 3d orbital in a high spin state  $\text{Mn}^{3+}$  has the theoretical spin moment of  $4 \mu_B$ , so the core polarisation contribution to the hyperfine field of 40 T is expected, which corresponds to the resonant frequency of 422 MHz. As was already mentioned in this chapter, anisotropic contributions are  $\vec{B}_{s-d}$ ,  $\vec{B}_{orb}$ ,  $\vec{B}_D$  and  $\vec{B}_T$ . The large anisotropy of the  $\text{Mn}^{3+}$  ion effective field observed cannot be explained solely by the anisotropy of the local contribution of dipolar fields ( $\vec{B}_D$ ) from magnetic neighbours. This anisotropy was found to be less than 0.2 T in the compound studied, whereas the observed anisotropy of the  $\text{Mn}^{3+}$  effective field is of 2 T. Also the anisotropy of  $\vec{B}_T$  is the most likely smaller. For example, in the iron garnet the anisotropy of  $\text{Fe}^{3+}$  at the distorted octahedral position was found to be of 0.2 T [Stepankova 2000]. Therefore the observed  $\text{Mn}^{3+}$  effective field anisotropy has to originate from the anisotropy of the  $\vec{B}_{orb}$  and/or  $\vec{B}_{s-d}$ .

The orbital field,  $\vec{B}_{orb}$  results from an unquenched orbital moment, which was confirmed to be nonzero in cubic manganese perovskites both by theoretical calculations (for  $\text{LaMnO}_3$  compound) [Solovyev 1997, Radwanski 2004] and experimentally by means of X-ray circular dichroism (for the series of Sr doped cubic perovskites) [Koide 2001]. The experimentally obtained values of the orbital magnetic moment were up to  $0.13 \mu_B$  (for  $\text{La}_{0.67}\text{Sr}_{0.33}\text{MnO}_3$ ) and that theoretically calculated for  $\text{LaMnO}_3$  was of  $0.24 \mu_B$  [Radwanski 2004]. From polarized neutron diffraction results on the  $\text{La}_{1.2}\text{Sr}_{1.8}\text{Mn}_2\text{O}_7$  compound the orbital moment was derived to be of  $0.35 \mu_B$  at 100 K [Argyriou 2002].

Assuming that the hyperfine field anisotropy comes solely from the anisotropy of the orbital moment and following Streever's calculations [Streever 1978, 1979] we obtained equation 7 which allowed us to derive the value of the orbital magnetic moment anisotropy:

$$\Delta\mu_L [\mu_B] = \frac{\Delta H_{eff}}{2\mu_B \langle r^{-3} \rangle (a.u.)^3} \quad (7)$$

where  $\Delta H_{eff}$  is the difference between values of the observed effective fields for  $\text{Mn}^{3+}$  (in cgs units),  $\langle r^{-3} \rangle$  is the average reciprocal cube of the radius of the 3d orbital, which amounts to 4.7897 [Watson 1963] and [a.u.] is the atomic unit. The obtained value of the orbital magnetic moment anisotropy,  $\Delta\mu_L$  for  $x=0.4$  and  $x=0.5$  compounds is close to  $0.04 \mu_B$ . Taking

the value of the spin-orbit coupling energy  $E_{SO} = \lambda LS$ , with  $\lambda = \zeta/2S$  ( $\zeta = 46$  meV [Van der Laan 1991] and  $S=2$ , for  $Mn^{3+}$  in the high spin state) one obtains  $E_{SO}$  of order of  $10^7$  erg/cm<sup>3</sup> while the observed magnetocrystalline anisotropy is of order of  $10^5$  erg/cm<sup>3</sup> [Renard 2003]. Thus, the observed anisotropy of the  $Mn^{3+}$  hyperfine field can not be attributed to the anisotropy of the orbital moment, which would correspond to unphysically high magnetocrystalline anisotropy.

Therefore, the main contribution to the hyperfine field anisotropy has to arise from  $\vec{B}_{S-d}$ , which is given by the equation 3 and calculated for the electrons on the  $3d$  orbital of the Mn ion (table 2). Assuming that the occupancy,  $\alpha$  of the  $x^2 - y^2$  or  $3z^2 - r^2$  orbitals in all the  $Mn^{3+}$  cations is the same and only the orientation of the magnetic moments varies from along the  $c$  axis to within the  $ab$  plane, this different orientation would result in an anisotropy of the spin dipolar field produced by the  $e_g$  electron. If we have two partly occupied  $3d$   $e_g$  orbitals one can write the following expression for  $\vec{B}_{S-d}$  produced by an electron on these orbitals:

$$B_{S-d}^{[100]} = \alpha B_{[100]}^{x^2-y^2} + (1-\alpha) B_{[100]}^{3z^2-r^2} \quad (8)$$

Similar equation can be written for  $B_{S-d}^{[001]}$ . Assuming the hyperfine field anisotropy as originating solely from the  $\vec{B}_{S-d}$  the  $\Delta B_{eff}$  can be obtained as:

$$\Delta B_{eff} = \alpha B_{[100]}^{x^2-y^2} + (1-\alpha) B_{[100]}^{3z^2-r^2} - \left[ \alpha B_{[001]}^{x^2-y^2} + (1-\alpha) B_{[001]}^{3z^2-r^2} \right] \quad (9)$$

Then one can easily derive  $\alpha$  as:

$$\alpha = \frac{\Delta B_{eff} - B_{[100]}^{3z^2-r^2} + B_{[001]}^{3z^2-r^2}}{B_{[100]}^{x^2-y^2} - B_{[100]}^{3z^2-r^2} - B_{[001]}^{x^2-y^2} + B_{[001]}^{3z^2-r^2}} \quad (10)$$

For the  $x=0.4$  compound one obtains  $\alpha=0.48$  and for  $x=0.5$   $\alpha=0.46$ , which indicates a slightly higher occupancy of the  $3z^2 - r^2$  orbital than the  $x^2 - y^2$  one. This finding does not agree with the results derived from magnetic Compton profiles [Li 2004], where at low temperatures  $\alpha$  for compound  $x=0.4$  was found to be of 0.78. One has to note that our calculation uses a value of the  $\vec{B}_{S-d}$  obtained for electrons in a free ion, not in the crystal. Moreover, as was mentioned earlier, there are also suggestions in the literature that the  $3z^2 - r^2$  orbital can have its occupation larger than the  $x^2 - y^2$  one [Argyriou 2002].

Unlike low Sr doped samples ( $0.3 \leq x \leq 0.5$ ) of bilayered manganese perovskites presented above, which were prepared as single crystals and were afterwards powdered, higher Sr doped compounds ( $0.5 \leq x \leq 1$ ) discussed in the section below, were prepared as powders by the solid state reaction method. Also all the results presented above were carried out on the spectrometer in Kraków and the results presented below on the Bruker Avance NMR spectrometer in Prague.

Fig. 16 presents normalised  $^{55}Mn$  zero field NMR spin echo spectra at 4.2 K of  $La_{2-2x}Sr_{1+2x}Mn_2O_7$  (for  $x=0.5$ ,  $x=0.62$  and  $x=0.68$ ) compounds. For samples with  $x=0.5$  and  $x=0.62$  the spectra presented are envelopes of several frequency swept spectra with excitation conditions optimal for several frequencies in order to take into account the possible differences in excitation conditions and also to reduce the influence of standing waves in the transmission line. For the sample with  $x=0.68$  two spectra are presented. The spectrum plotted with the solid line is an envelope of two measurements with optimal excitation conditions at 335 MHz ( $Mn^{4+}$  in FMI regions) and 380 MHz (the DE line). The spectrum plotted with dashed line is obtained for optimal excitation conditions at 290 MHz ( $Mn^{4+}$  in AFI regions).

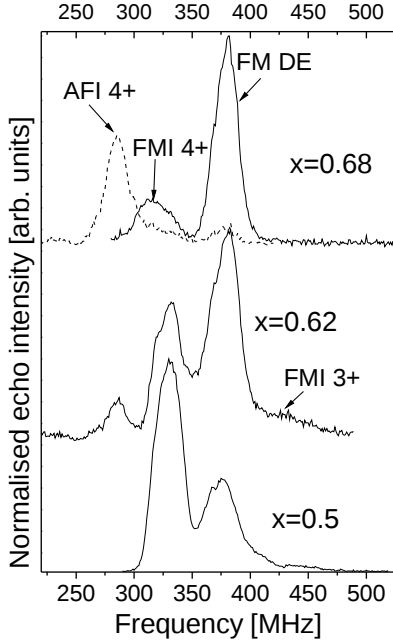


Fig. 16.  $^{55}\text{Mn}$  zero field NMR spin echo spectra at 4.2 K of  $\text{La}_{2-2x}\text{Sr}_{1+2x}\text{Mn}_2\text{O}_7$  (for  $x=0.5$ ,  $x=0.62$  and  $x=0.68$ ). Abbreviations used denote: AFI 4+ ( $\text{Mn}^{4+}$  ions in antiferromagnetic insulating regions), FMI 4+ ( $\text{Mn}^{4+}$  ions in ferromagnetic insulating regions), FMI 3+ ( $\text{Mn}^{3+}$  ions in ferromagnetic insulating regions), FM DE ( $\text{Mn}^{3+/4+}$  ions in ferromagnetic metallic regions where the double exchange interaction is effective).

Starting from  $x=0.5$  we see that the spectrum presented in Fig. 16 is different from the spectrum for sample of the same doping, but prepared as single crystal and powdered afterwards (see Fig. 15b, the bottom plot for pulse spacing 10  $\mu\text{s}$ ). Let us analyse possible reasons of observed differences. First of all, the preparation process of both samples is different, also some differences in the frequency response between the two spectrometers used, i.e. the Bruker Avance spectrometer

in Prague and the spectrometer in Krakow cannot be excluded. Despite differences in relative intensities of observed resonance lines of both spectra, for both samples the same lines are observed i.e. the line arising from  $\text{Mn}^{4+}$  ions in FMI regions, the DE line and the line originating from  $\text{Mn}^{3+}$  ions in FMI regions due to the phase segregation in the compounds studied. For  $x=0.5$  Sr doped sample prepared as a powder (results presented in this chapter) these lines are observed at 329.47 MHz (31.23 T), 375.85 MHz (35.63 T) and above 400 MHz for the FMI  $\text{Mn}^{4+}$  line, the FM DE line and FMI  $\text{Mn}^{3+}$  signals, respectively.

In the  $x=0.62$  compound, besides lines observed for  $x=0.5$ , i.e. the  $\text{Mn}^{4+}$  line in FMI regions at 330 MHz, the DE line at 378 MHz and weak signals from  $\text{Mn}^{3+}$  ions in FMI regions above 400 MHz, an additional line centred at 284 MHz is observed. In the literature presenting the  $^{55}\text{Mn}$  NMR results on manganese perovskites the lines below 300 MHz are ascribed to the Mn ions in antiferromagnetic insulating (AFI) regions [Allodi 1997, Kapusta 2000, Savosta 2000]. The resonant frequency and corresponding effective field,  $\bar{B}_{\text{eff}}$  is lower in the case of the antiferromagnetic neighbourhood, because the sign of the transferred hyperfine field depends on the orientation of neighbouring spins, therefore the effective field for AF coupled neighbours is of opposite sign compared with that in the FM neighbourhood. This can be seen, if one writes the formula for the effective field in the following way:

$$B_{\text{eff}}^i = \frac{2\pi}{\gamma} g\mu_B \left( A^i \langle S^i \rangle + \sum_j B^j \langle S^j \rangle \right) + B_0 \quad (11)$$

where  $\langle S^i \rangle$  and  $\langle S^j \rangle$  are on-site and nearest neighbour electron spins,  $A^i$  and  $B^j$  are respective hyperfine couplings and  $B_0$  is the external field.

The distinction, which line is due to antiferromagnetic or ferromagnetic structure is not trivial, however it is possible with the measurements in the applied magnetic field. As was already mentioned, if spins are coupled ferromagnetically, the resonant frequency shifts

towards lower frequencies due to the fact that the hyperfine field is dominant and antiparallel to the manganese moment. On the contrary, for an antiferromagnet with a low magnetocrystalline anisotropy, or easy magnetisation direction of the easy-plane type, as expected for the compounds in the doping range  $0.5 \leq x < 1$ , the sublattice magnetizations will tend to align perpendicularly to the applied field because the perpendicular susceptibility is larger than the parallel one. Hence, the resonant frequency corresponding to the effective field, which is a vector sum of the hyperfine field and a much smaller applied field, changes only a little comparing to that at no applied field [Allodi 1997]. In such a situation the AF line only broadens without noticeable shifting in frequency [Allodi 1998].

Fig. 17 presents field measurements of  $\text{La}_{0.76}\text{Sr}_{2.24}\text{Mn}_2\text{O}_7$  ( $x=0.62$ ) compound at 0 T, 1 T and 1.5 Tesla at temperature 4.2 K. As expected for the signal from the antiferromagnetically ordered magnetic moments the line at 284 MHz does not shift in the applied field in contrast to the DE line at 378 MHz which shifts towards lower frequencies as expected for the ferromagnetically ordered moments. The resonant frequency of the DE line shifts to 367 MHz at 1 Tesla which agrees well with the value of the gyromagnetic ratio of  $^{55}\text{Mn}$ , which is 10.553 MHz/T (11 MHz drop corresponds to decrease of the effective field by 1.05 T). The  $\text{Mn}^{4+}$  FMI line also shifts to lower frequencies in the applied field but due to its overlapping with other lines one can not determine its exact shift in applied field.

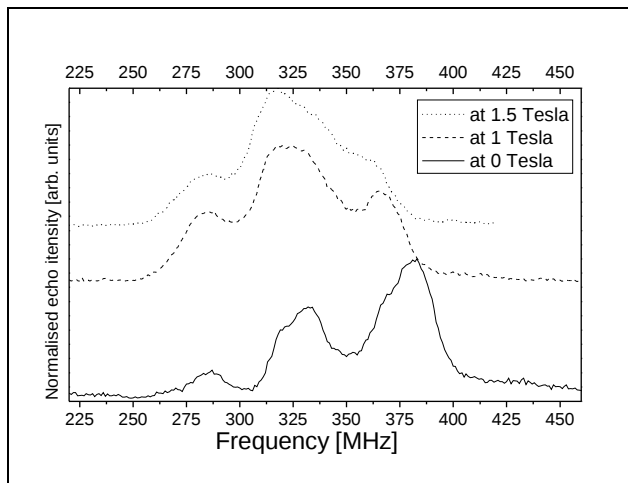


Fig. 17. The  $^{55}\text{Mn}$  NMR spin echo spectra at 4.2 K for  $\text{La}_{0.76}\text{Sr}_{2.24}\text{Mn}_2\text{O}_7$  ( $x=0.62$ ) compound at 0 T, 1 T and 1.5 Tesla.

Second indication of the type of the magnetic ordering is the comparison of the enhancement factors,  $\eta$ . The enhancement factor for an antiferromagnet,  $\eta_{AF}$  (in the most effective case: external field in the easy plane, sublattice magnetizations perpendicular to the external field) is typically between 10 and 100, which is few orders of magnitude smaller than the enhancement factor for a ferromagnet,  $\eta_F$ . In the case of the  $x=0.62$  compound optimal excitation conditions for the DE line were: pulse length 1  $\mu\text{s}$  while for the AF line at 284 MHz pulse length used was 5  $\mu\text{s}$  and pulse amplitude (which corresponds to the rf field) was 10 times larger than for the DE line. Since the enhancement factor is inversely proportional to the product of the optimal pulse length and radio frequency field one obtains that  $\eta_{AF}$  is of 50 times smaller than  $\eta_{DE}$  (the enhancement factor in the ferromagnetically ordered DE regions).

One has to keep in mind that the enhancement factor in the ferromagnetic material is much smaller for nuclei in domains than for nuclei in domain walls. However the possibility that the signal at 280-290 MHz comes from nuclei in ferromagnetically ordered domains (smaller enhancement factor) can be excluded since in the applied field such line should also shift towards lower frequencies, which is not the case.

In Fig. 16 also two frequency swept spectra for the  $x=0.68$  compound are presented. As was already mentioned the spectrum plotted with the solid line is an envelope of two measurements with optimal excitation conditions at 335 MHz ( $\text{Mn}^{4+}$  in FMI regions) and 380

MHz (the DE line). The spectrum plotted with the dashed line is for optimal conditions at 290 MHz ( $\text{Mn}^{4+}$  in AFI regions). Separate spectra are presented due to much different optimal excitation conditions (much different enhancement factors) and the overlap of the AFI and FMI  $\text{Mn}^{4+}$  lines.

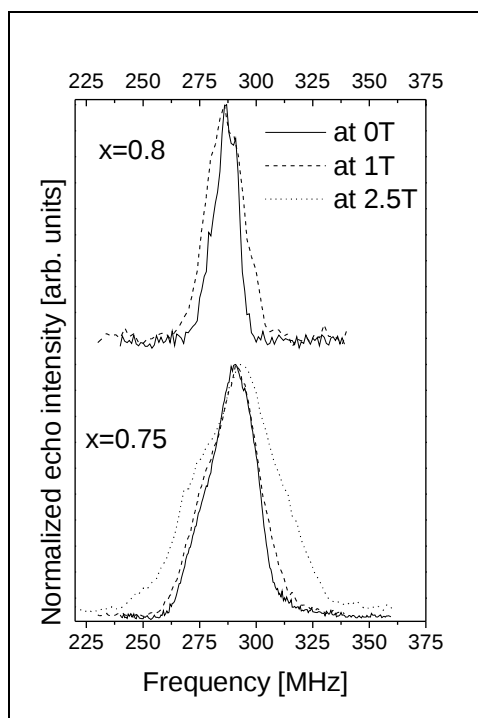


Fig. 18. The  $^{55}\text{Mn}$  NMR spin echo spectra at 4.2 K of  $\text{La}_{0.5}\text{Sr}_{2.5}\text{Mn}_2\text{O}_7$  ( $x=0.75$ ) at 0 T (solid line), 1 T (dashed line) and 2.5 T (dotted line) and of  $\text{La}_{0.4}\text{Sr}_{2.6}\text{Mn}_2\text{O}_7$  ( $x=0.8$ ) at 0 T (solid line) and 1 T (dashed line).

The  $^{55}\text{Mn}$  NMR spin echo spectra of  $\text{La}_{0.5}\text{Sr}_{2.5}\text{Mn}_2\text{O}_7$  ( $x=0.75$ ) and  $\text{La}_{0.5}\text{Sr}_{2.5}\text{Mn}_2\text{O}_7$  ( $x=0.8$ ) at 0 T and at the applied field 1 T and 2.5 T measured at 4.2 K are presented in Fig. 18. For both compounds at no applied field only one line is observed, centred at 290 MHz and 287 MHz for the  $x=0.75$  and  $x=0.8$  compound respectively. Also in the applied field one line is observed and it does not shift, which indicates that the line is due to  $\text{Mn}^{4+}$  in antiferromagnetically ordered regions.

The enhancement factor for  $x=0.75$  and  $x=0.8$  compounds is smaller than for  $\text{Mn}^{4+}$  AFI line in  $x=0.62$  and  $x=0.68$  compounds. Even with the first pulse of the spin-echo sequence 10  $\mu\text{s}$  long and 300 Watt pulse amplifier, which was used for all measurements presented in this chapter, carried out on the Bruker spectrometer in Prague, we were unable to reach maximum of the signal versus pulse attenuation scan. This also influenced the quality of the frequency swept spectra, due to a larger influence of the standing waves at the non-optimal excitation conditions. Usually, at the applied field the optimal excitation conditions require more power (and/or longer pulses), which in our case means that we are more away from optimal conditions in the measurements carried out at the applied field than in the measurements at 0 T. The necessity for using very long pulses at the full power clearly indicates that the enhancement factor  $\eta$  for  $x=0.75$  and  $x=0.8$  compounds is smaller than in the case of the AFI line for  $x=0.62$  and  $x=0.68$  compounds. This indicates a more perfect AF order or/and a higher magnetocrystalline anisotropy in the former compounds. In fact, this is consistent with the magnetic structures determined by the neutron diffraction [Mitchell 2001]. The compound with  $x=0.62$  has ferromagnetically ordered planes coupled antiferromagnetically (4 neighbours FM coupled and 2 AF coupled), while  $x=0.75$  and  $x=0.8$  compounds have ferromagnetically ordered "rods" (2 neighbours coupled FM and 4 AF coupled).

Both, the small enhancement factor and a lack of shift of the resonance line at the applied field indicate that the observed signal is due to antiferromagnetically ordered regions, similarly to the  $x=0.68$  compound. Also magnetisation versus applied field curves were measured and they did not show any ferromagnetic contribution.

We failed to observe any NMR spin-echo signal from the  $x=1$  compound (all Mn next neighbours coupled antiferromagnetically). Attempts in the frequency range 200-350 MHz with excitation conditions similar to those used in the case of  $x=0.75$  and  $x=0.8$  compounds both at no applied field and at 1 T did not succeed and no spin echo signal could be observed.

## 6. Conclusions

The  $^{55}\text{Mn}$  and  $^{139}\text{La}$  NMR study of “cubic” and bilayered perovskites doped with Sr or Ca, which exhibit ferromagnetic insulating/metallic or antiferromagnetic insulating behaviour, lead to the following findings:

- The phase segregation is observed in all the compounds studied and it does not depend on the dimensionality of the compounds and the type of dopant (Sr or Ca). It appears on both sides of the phase diagram, below  $x=0.15$  Sr doping (in “cubic” perovskites) and above  $x=0.5$  (in bilayered perovskites). It is observed in the  $^{55}\text{Mn}$  spectra as well as in the  $^{139}\text{La}$  spectra of low doped “cubic” compounds.
- Temperature measurements of  $\text{La}_{0.875}\text{Sr}_{0.125}\text{MnO}_3$  compound reveal that ferromagnetic metallic regions exist above the bulk  $T_C$  indicating existence of ferromagnetic polarons above this temperature. They also reveal that the magnetic coupling in the FMI regions is weaker than in the FMM ones.
- The  $\text{Mn}^{4+}$  signals range from below 300 MHz in the case of  $\text{Mn}^{4+}$  ions ordered antiferromagnetically, to 330 MHz for  $\text{Mn}^{4+}$  ions in FMI regions.
- Multi-line signals are observed for  $\text{Mn}^{3+}$  ions, indicating their considerable hyperfine field anisotropy. They range from 400 MHz to 550 MHz. In bilayered perovskites (for compounds with  $0.35 \leq x \leq 0.5$ ) the occupation of 3d  $e_g$  orbitals was derived from the hyperfine field anisotropy and a higher occupation of the  $3z^2 - r^2$  orbital was concluded.
- The frequency swept spectra and the frequency dependence of the spin-spin relaxation time of the  $\text{La}_{0.85}\text{Sr}_{0.15}\text{MnO}_3$  compound at 4.2 K and at 77 K show the influence of the Suhl-Nakamura interaction between  $^{55}\text{Mn}$  nuclear moments within the DE-driven metallic-like regions. These regions in  $\text{La}_{0.85}\text{Sr}_{0.15}\text{MnO}_3$  are found to be larger than 10 nm in size while in  $\text{La}_{0.875}\text{Sr}_{0.125}\text{MnO}_3$  they are smaller.
- Nanoparticle powders of  $\text{La}_{0.75}\text{Sr}_{0.25}\text{MnO}_3$  show a degradation of magnetic properties with decreasing of the average grain size. Signals from ferromagnetic metallic grain interiors and ferromagnetic insulating outer layers of grains are identified.
- In heavily doped bilayered perovskites with  $0.5 \leq x \leq 0.68$  signals from both antiferromagnetic and ferromagnetic regions are observed, also in the compound with no long range magnetic order ( $x=0.68$ ). For compounds with  $x=0.75$  and  $x=0.8$  only signals from antiferromagnetic regions are detected. Also magnetisation measurements show no ferromagnetic contribution in these two compounds.

## 7. List of publications

### Publications related to the thesis:

1. J. Przewoźnik, Cz. Kapusta, J. Żukrowski, K. Krop, M. Sikora, D. Rybicki, D. Zając, B. Sobanek, C.J. Oates, P.C. Riedi “*On the strength of the double exchange and superexchange interactions in  $La_{0.67}Ca_{0.33}Mn_{1-y}Fe_yO_3$  – an NMR and Mössbauer study*”, *Physica Status Solidi B* **243**, 259 (2006)
2. D. Rybicki, M. Sikora, Cz. Kapusta, P.C. Riedi, Z. Jirak, K. Knizek, M. Marysko, E. Pollert and P. Veverka, “*The  $^{55}Mn$  NMR study of the  $La_{0.75}Sr_{0.25}MnO_3$  nanoparticles*”, *Physica Status Solidi C* **3**, 155 (2006)
3. D. Rybicki, Cz. Kapusta, P.C. Riedi, C.J. Oates, M. Sikora, D. Zając, J.M. De Teresa, C. Marquina M.R. Ibarra, „*A  $^{55}Mn$  NMR study of  $La_{0.33}Nd_{0.33}Ca_{0.34}MnO_3$  with  $^{16}O$  and  $^{18}O$* ”, *Acta Phys. Polon. A* **105**, 183 (2004)
4. C.J. Oates, Cz. Kapusta, P.C. Riedi, M. Sikora, D. Zając, D. Rybicki, C. Martin, C. Yaicle, A. Maignan „*An NMR study of  $Pr_{0.5}Ca_{0.5}Mn_{0.97}Ga_{0.03}O_3$* ”, *Acta Physica Polonica A* **105**, 189 (2004)
5. Cz. Kapusta, D. Rybicki, P.C. Riedi, C.J. Oates, D. Zając, M. Sikora, C. Marquina, M.R. Ibarra, „*NMR study of layered manganite  $La_{1.4}Sr_{1.6}Mn_2O_7$* ”, *Journal of Magnetism and Magnetic Materials*, **272-276**, 1759 (2004)

### Other publications:

1. M. Sikora, D. Zając, Cz. Kapusta, M. Borowiec, C.J. Oates, V. Procházka, D. Rybicki, J.M. De Teresa, C. Marquina and M.R. Ibarra, „*Evidence of unquenched Re orbital magnetic moment in  $AA'FeReO_6$  double perovskites*”, *Applied Physics Letters* **89**, 62509 (2006)
2. M. Sikora, Cz. Kapusta, K. Knížek, Z. Jiráček, C. Autret, M. Borowiec, C. J. Oates, V. Procházka, D. Rybicki, and D. Zając „*X-ray absorption near-edge spectroscopy study of Mn and Co valence states in  $LaMn_{1-x}Co_xO_3$ ,  $x=0-1$* ”, *Physical Review B* **73**, 94426 (2006)
3. M. Sikora, C. Kapusta, K. Knížek, Z. Jiráček, C. Autret, M. Borowiec, C.J. Oates, V. Procházka, D. Rybicki and D. Zając “*XANES study of  $LaMn_{1-x}Co_xO_3$  series*”, *Hasylab Annual Report, DESY, Hamburg* (2005)
4. C.J. Oates, M. Borowiec, C. Kapusta, D. Rybicki, M. Sikora, W. Szczerba, R. Ruiz-Bustos, P.D. Battle, M.J. Rosseinsky and E. Welter, “*XAS study of Ru doped  $n=1,2$  Ruddlesden-Popper manganites*” *Hasylab Annual Report, DESY, Hamburg* (2004)

5. M. Sikora, D. Zając, M. Borowiec, C. J. Oates, V. Prochazka, D. Rybicki, Cz. Kapusta "XMCD study of rhenium orbital moment in magnetoresistive double perovskites" Hasylab Annual Report, DESY, Hamburg (2004)
6. D. Zając, Cz. Kapusta, P.C. Riedi, M. Sikora, C.J. Oates, D. Rybicki, J.M. De Teresa, D. Serrate, C. Marquina, M.R. Ibarra, „NMR study of  $(\text{Sr},\text{Ba},\text{La})_2\text{Fe}_{1+y}\text{Mo}_{1-y}\text{O}_6$  double perovskites”, Acta Physica Polonica A **106**, 759 (2004)
7. D. Zając, Cz. Kapusta, P.C. Riedi, M. Sikora, C.J. Oates, D. Rybicki, D. Serrate, J.M. De Teresa M.R. Ibarra, „NMR and X-MCD study of  $\text{Sr}_{1-3x}\text{Ba}_{1+x}\text{La}_{2x}\text{FeMoO}_6$ ”, Journal of Magnetism and Magnetic Materials, **272-276**, 1756 (2004)
8. M. Sikora, Cz. Kapusta, D. Zając, W. Tokarz, C.J. Oates, M. Borowiec, D. Rybicki, E. Goering, P. Fisher, G. Shütz, J.M. De Teresa, M.R. Ibarra, „XMCD magnetometry of CMR perovskites  $\text{La}_{0.67-y}\text{Re}_y\text{Ca}_{0.33}\text{MnO}_3$ ”, Journal of Magnetism and Magnetic Materials, **272-276** (2004) 2148
9. D. Zając, M. Sikora, C.J. Oates, M. Borowiec, D. Rybicki, Cz. Kapusta, J. Blasco, J.M. De Teresa, C. Marquina, M.R. Ibarra, „X-MCD study of double perovskites  $(\text{Sr},\text{Ba},\text{Ca})_2\text{FeReO}_6$ ” Hasylab Annual Report 2003, DESY, Hamburg (2003)
10. D. Zając, Cz. Kapusta, M. Sikora, D. Rybicki, M. Borowiec, E. Welter, „XANES and X-MCD study of double perovskites  $(\text{Sr},\text{Ba},\text{La})_2\text{FeMoO}_6$ ”, Hasylab Annual Report 2002, DESY, Hamburg (2002)
11. M. Sikora, Cz. Kapusta, D. Zając, M. Borowiec, D. Rybicki, J. Żukrowski, M. Kapusta, P. Fischer, E. Goering, G. Schütz, E. Welter, „X-MCD magnetometry of mixed valence manganites  $(\text{La},\text{Re})_{0.67}\text{Ca}_{0.33}\text{MnO}_3$  ( $\text{RE}=\text{Nd},\text{Tb}$ )”, Hasylab Annual Report 2001, DESY, Hamburg (2001)

## 8. References

- Abragam A., Bleaney B., *Electron paramagnetic resonance of transition ions* (Clarendon Press, Oxford, 1970), p. 689
- Algarabel P.A., et al., *Phys. Rev. B* **67**, 134402 (2003)
- Allodi, G., et al., *Phys. Rev. B* **56**, 6036 (1997)
- Allodi G., De Renzi R., Licci F., Pieper M. W., *Phys. Rev. Lett.* **81**, 4736 (1998)
- Argyriou D.N., Brown P. J., Gardner J., Heffner R. H., *Phys. Rev. B* **65**, 214431 (2002)
- Asano S., Ishida S., *J. Magn. Magn. Mater.* **70**, 187 (1987)
- Bibes M., et al., *Appl. Phys. Lett.* **82**, 928 (2003)
- Dabrowski B., et al., *Phys. Rev. B.* **60**, 7006 (1999)
- Dagotto E., et al., *Phys. Rep.* **344**, 1 (2001)
- Davis J. H., Searle C. W., *Phys. Rev. B* **9**, 323 (1974)
- Davis J.H. and Searle C.W., *Phys. Rev. B* **14**, 2126 (1976)
- Hennion M., et al., *Phys. Rev. Lett.* **81**, 1957 (1998)
- Hone D., Jaccarino V., Ngwe T. and Pincus P., *Phys. Rev.* **186**, 291 (1969)
- Jonker G. H. and van Santen J. H., *Physica* **16**, 337 (1950)
- Jonker G. H., *Physica* **22**, 707 (1956)
- Kapusta Cz., et al., *J. Phys.: Condens. Matter* **11**, 4079 (1999)
- Kapusta Cz., Riedi P.C., Sikora M., Ibarra M.R., *Phys. Rev. Lett.* **84**, 4216 (2000)
- Kapusta Cz., Riedi P.C., Kocemba W., Ibarra M.R., Coey J.M.D., *J. Appl. Phys.* **87**, 7121 (2000)
- Kapusta Cz. and Riedi P., *Hyperfine Interact.* **133**, 127 (2001)
- Koide T. et al., *Phys. Rev. Lett.* **87**, 246404 (2001)
- Kumagai K., et al., *Phys. Rev. B* **59**, 97 (1999)

- Kusters R.M., Singleton J., Keen D.A., McGreevy R., Hayes W., *Physica B* **155**, 362 (1989)
- Leung L.K. and Morrish A.H., *Phys. Rev. B* **15**, 2485 (1977)
- Li Yinwan et al., *Phys. Rev. Lett.* **93**, 207206 (2004)
- Lord J.S., Riedi P.C., *Meas. Sci. Technol.* **6**, 149 (1995)
- Matsumoto G., *J. Phys. Soc. Jpn.* **29**, 615 (1970)
- Mitchell J. F., et al., *J. Phys. Chem* **105** (2001)
- Nakamura T., *Progr. Theoret. Phys., Kyoto*, **20**, 542 (1958)
- Novak P., *Acta Physica Polonica* **105**, 57 (2004)
- Papavassiliou G., et al., *Phys. Rev. B* **55**, 15000 (1997)
- Papavassiliou G., et al., *Phys. Rev. B* **59**, 6390 (1999)
- Papavassiliou G., et al., *Phys. Rev. B* **58**, 12237 (1998)
- Papavassiliou G., et al., *Phys. Rev. Lett.* **84**, 761 (2000)
- Papavassiliou G., Belesi M., Fardis M. and Dimitropoulos C., *Phys. Rev. Lett.* **87**, 177204 (2001)
- Radwański R.J., Ropka Z., *J. Magn. Magn. Mater.* **272**, 259 (2004)
- Renard J.-P., Anane A., *Mat. Sci. Eng. B* **63**, 22 (1999)
- Renard J.-P. and Velázquez M., *Eur. Phys. J. B* **34**, 41 (2003)
- Riedi P.C., Lord J.S., in *Interstitial Intermetallic Alloys*, NATO ASI series, Vol. **281**, F. Grandjean, G.J. Long, K.H.J Buschow eds. (Kluwer, Dordrecht 1994)
- Rybicki D., et al., *Acta Physica Polonica* **105**, 183 (2004)
- Salafranca J. and Verges J. A., *Phys. Rev. B* **74**, 184428 (2006)
- Savosta M., Borodin V. A., Novak P., *Phys. Rev. B* **59**, 8778 (1999)
- Savosta M., et al., *Phys. Rev. B* **62**, 9532 (2000)
- Savosta M., M., Novak P., *Phys. Rev. Lett.* **87**, 137204 (2001)
- Savosta M. M., et al., *Phys. Rev. B* **69**, 24413 (2004)
- Solovyev I., *Phys. Rev. B* **55**, 8060 (1997)
- Stepankova H., Kohout J., Englich J. and Novak P., *Hyperfine Interactions* **131**, 3 (2000)
- Streever R. L., *Phys. Lett.* **65A**, 360 (1978)
- Streever R. L., *Phys. Rev. B* **19**, 2704 (1979)
- Suhl H., *Phys Rev* **109**, 606 (1958)
- Turov E.A., Pietrow M.P., *Jądrowy rezonans magnetyczny w ferromagnetykach i antyferromagnetykach*, PWN, (1970)
- van der Laan G., *J. Phys. Condens. Matter* **3**, 7443 (1991)
- van Santen J. H., and Jonker G. H, *Physica* **16**, 599 (1950)
- Watson R.E., *Magnetism* ed. G.T. Rado, H. Suhl, Vol. IIA, page 291, Academic Press (1963)
- Weisman I. D., Swartzendruber L. J., and Bennett L. H., in *Technique of Metal Research*, edited by E. Passaglia (Wiley, New York, 1973) Vol. VI, page 360
- Xiong X. et al, *Phys. Rev. B* **60**, 10186 (1999)
- Xu, S., et al., *J.Phys. Soc. Japan* **72**, 709 (2003)
- Yakubowskii A., et al., *Phys. Rev. B* **62**, 5337 (2000)
- Zener C., *Phys. Rev.* **81**, 440 (1951)